Inorganic Chemistry

Article

pubs.acs.org/IC

Thermal Decomposition and Recovery Behaviors of Layered Gadolinium Hydroxychloride

Seoung-Soo Lee,[†,∥] Byung-Il Lee,[§,∥] Seung-joo Kim,[†,‡] Song-Ho Byeon,*[,§] and Jun-Kun Kang*[,†]

[†]Institute of NT-IT Fusion Technology, Ajou University, Suwon 443-749, Korea

[‡]Department of Chemistry, Division of Energy Systems Research, Ajou University, Suwon, 443-749, Korea

[§]Department of Applied Chemistry, College of Applied Science, Kyung Hee University, Gyeonggi 446-701, Korea

Supporting Information

ABSTRACT: The thermal behavior of gadolinium hydroxychloride ($Gd_2(OH)_5Cl{\cdot}nH_2O$, LGdH) has been closely studied to provide the important factors that should be considered for its high temperature applications. Combined analyses of thermogravimetry-differential scanning calorimetry-mass spectrometry (TG-DSC-MS) showed that, under atmospheric air with a considerable amount of water, the decomposition of LGdH to Gd_2O_3 is completed at 1050 °C. However, in either dry air or Ar gas, the transformation continued up to around 1300 °C. Thus, the thermal decomposition of LGdH was more influenced by H_2O than by O_2. FT-IR spectra and X-ray diffraction (XRD) patterns were used to study LGdHs calcined at high temperatures (up to at least 600 °C). Calcined LGdH's ability to intercalate anions into the interlayer space could be recovered by the reconstruction of intralayer structure through rehydration and rehydroxylation. These processes were significantly accelerated at elevated temperatures. The recovery behavior of LGdH was examined in different anionic solutions at different temperatures.

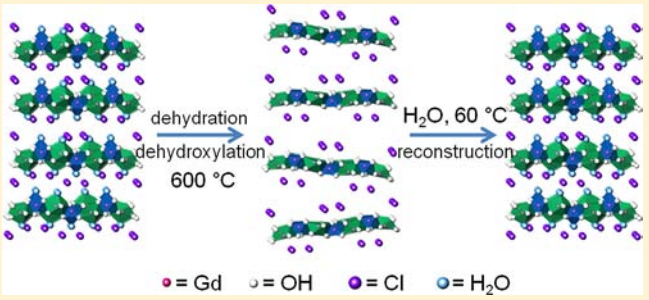

1. INTRODUCTION

Layered double hydroxides (LDHs) are able to have flexible layer compositions. The anions intercalated in their interlayers allow a wide variety of applications in diverse fields.[1] In contrast, rare-earth cations are not readily incorporated into the hydroxide layer, even though chelate complexes of La^{3+}, Eu^{3+}, and Gd^{3+} have been intercalated into LDH galleries.[2] Compounds of pure cationic rare-earth layers pillared by rigid organic anions have recently been reported.[3] Successive researches performed by several groups have developed a series of layered rare-earth hydroxides (LRHs) with the general formula, $RE_2(OH)_5X{\cdot}nH_2O$, where RE = rare-earths and X = interlayer organic or inorganic anions.[4] LRHs are structurally similar to LDHs and consist of positively charged rare-earth hydroxide layers with exchangeable, charge-balancing anions in the interlayer space. This family of layered materials has received attention for its potential application in luminescence films.[5] Overall characteristics of LRHs refer to the recent review.[6]

As an LRH, $Gd_2(OH)_5Cl{\cdot}nH_2O$ (LGdH) is of particular interest because of the highly paramagnetic behavior ($S = 7/2$) of Gd^{3+}, large water-accessible surface area, and capacity to incorporate functional molecules between layers. The magnetic resonance (MR) relaxation properties of LGdH suspensions were previously examined, and their potential utility as positive contrast agents for T_1 weighted MR imaging was proposed in our previous report.[7] A colloid of surface-modified LGdH layers doped with Eu^{3+} ions (LGdH:Eu) demonstrated effectiveness as a dual imaging agent in cellular labeling for both fluorescent and MR imaging.[8] In addition, the LGdH lattice can be constructed by grafting functional groups onto gadolinium hydroxocation nanosheets.[9] A hierarchical superstructure is also constructed by the self-assembly of gadolinium hydroxocation layers and polyoxomolybdate anions, which exhibits a unique photoluminescence property.[10] Such flexible assembly behaviors provide this family of layered materials, including LGdH, with a wide range of possible applications in future research.

Apart from their potential as contrast agents and luminescence materials, LRHs have revealed high activity as heterogeneous catalyst for green chemistry.[3] Rare-earth catalysts are increasingly used in organic and energy conversion reactions.[11] Because of this, many interests have to be addressed to endow LRHs with great capability for catalysts or catalytic supporting materials. An in-depth understanding of the LRH family could suggest the most appropriate direction at the current stage of study for their applications. In this work, the thermal decomposition behavior of $Gd_2(OH)_5Cl{\cdot}nH_2O$ was closely investigated using the combined analytical method of thermogravimetry-differential scanning calorimetry-mass spectrometry (TG-DSC-MS). The variation of FT-IR spectra induced upon heating LGdH was explained in terms of mutual interactions between μ_3-OH bonds, which are typically observed as fine structures, and water molecules in the

Received: May 30, 2012
Published: September 10, 2012

interlayer space. More interestingly, rehydration and rehydroxylation in appropriate aqueous solutions can recover the ability of LGdHs calcined at high temperatures to intercalate organic and inorganic anions into their interlayer galleries. Herein, we report the important thermal and recovery behaviors of LGdH that should be considered for high temperature applications. Those specific applications could be exploited for general applications of the extended LRH family.

2. EXPERIMENTAL SECTION

2.1. Preparation of $Gd_2(OH)_5Cl{\cdot}nH_2O$ (LGdH). All chemicals were supplied by Aldrich and were used without further purification. First, KOH solution (0.1 M) was added dropwise to $GdCl_3{\cdot}6H_2O$ solution (0.05 M) with vigorous stirring at room temperature (RT). This solution was maintained at 60 °C for 12 h and then refluxed with stirring for 24 h. The precipitate was then collected by a centrifuge and washed with deionized water. The resulting solid product, LGdH, was dried and stored in a desiccator.

2.2. Thermal Decomposition of LGdH. The thermogravimetric (TG) curve of LGdH was recorded at the heating rate of 5 °C/min from RT to 1300 °C. Data was collected in atmospheric air, dry air (99.999%), and Ar (99.999%) gas. The calcined products were obtained at various temperatures for X-ray diffraction (XRD) analyses. After reaching the target temperatures, the furnace was programmed to power down for natural cooling. For convenience, these samples are labeled LGdH-T (e.g., LGdH-250 is the sample calcined at 250 °C). The pristine sample is denoted by LGdH or LGdH-RT (RT: room temperature).

Simultaneous thermogravimetry-differential scanning calorimetry-mass spectrometry (TG-DSC-MS) analysis for LGdH was carried out from RT to 1300 °C under dry air flow using a TG-DSC instrument (Netzsch STA 409 PC) equipped with a mass spectrometer (QMS 403C). The temperature-programmed heating rate was 5 °C/min, and the flow rate of dry air was 50 mL/min.

2.3. Recovery of Intercalation Ability of Calcined LGdHs. To investigate the recovery of intercalation ability, exchange-reactions of calcined LGdHs were carried out with organic anions. In a typical reaction, LGdH powders (0.25 g) calcined at 350, 450, and 600 °C were dispersed into an aqueous anionic solution containing a 3-fold molar excess of octanesulfonate sodium salt ($C_8H_{17}SO_3Na$). The possible rehydroxylation of calcined LGdH and the successive ion-exchange reactions between Cl^- and sulfonate anion in the interlayer galleries of LGdH were performed at both RT and 60 °C in air while stirring for 24 and 18 h, respectively. The resulting precipitates were recovered by filtration, washed with water, and dried at 40 °C for one day.

2.4. Effect of Counteranions in Solution on the Reconstruction of Calcined LGdH Layers. For the rehydration and rehydroxylation of calcined LGdHs in various conditions, LGdH (0.25 g) calcined at 450 and 600 °C were added to 30 mL of deionized water or aqueous solutions of NaCl (1.0 M) and $NaNO_3$ (1.0 M). These suspensions were kept at RT for 24 h and at 60 °C for 18 h while stirring. The precipitate was filtered, washed with water, and dried at 40 °C in air.

2.5. Characterizations. XRD patterns of LGdH and its calcined products were recorded with a Rigaku DMAX-2200PC diffractometer using Ni-filtered Cu–Kα radiation. Infrared spectra over a range of 400–4000 cm^{-1} were obtained on a Thermo Scientific Nicolet iS10 FT-IR spectrophotometer using the KBr pellet technique. To make pellets, pristine LGdH (1.0 mg) and heat treated samples were diluted with IR-grade KBr powder (200 mg) and subjected to a pressure of 10 tons.

3. RESULTS AND DISCUSSION

The structure of $Gd_2(OH)_5Cl{\cdot}nH_2O$ is schematically represented in Figure 1, where positively charged gadolinium hydroxocation ($[Gd_2(OH)_5{\cdot}nH_2O]^+$) layers and charge-compensating chloride anion (Cl^-) layers are alternately arranged.

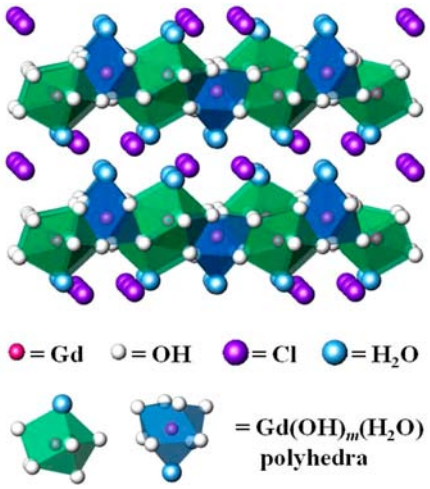

Figure 1. Ideal structure of $Gd_2(OH)_5Cl{\cdot}nH_2O$. The gadolinium atoms are coordinated by intralayer μ_3-hydroxyl groups and one interlayer water molecule. Eight- and nine-coordinated polyhedra are represented by green and blue, respectively.

Eight- and nine-coordinated $Gd(OH)_m(H_2O)$ (m = 7 and 8, respectively) polyhedra are linked with one another by intralayer μ_3-OH groups.

3.1. Thermal Decomposition Behavior of LGdH. In Figure 2a, the XRD pattern of LGdH is compared with those after heated at various temperatures in atmospheric air. The formation of well crystallized $Gd_2(OH)_5Cl{\cdot}nH_2O$ (LGdH-RT) with unit cell parameters of a = 12.81(1) Å, b = 7.21(4) Å, and c = 8.76(6) Å agrees with previous reports.[4e,7] At RT, LGdH shows well-developed (00l) reflections typical for the layered structure along with some non-(00l) reflections. As displayed in Figure 2a, the basal spacing of LGdH gradually increases from 8.76 Å to ~9.30 Å with heating up to 700 °C. Non-(00l) reflections associated with the intralayer (ab-plane) structure vary significantly after heating at 250 °C. Such a thermal behavior in atmospheric air is similar to previous observation.[12]

In contrast to the interlayer waters in layered double hydroxides, the water molecules in the gallery of LGdH are essentially included in the coordination polyhedra of Gd^{3+} ions in the layers. A slight expansion of basal spacing is likely attributed to the layer deformation due to dehydration and dehydroxylation. The formation of Gd_2O_3 is initiated around 600 °C but (00l) reflections from layered structure are maintained.[13] When LGdH is calcined at 750 °C, Gd_2O_3 becomes the main phase and some faint peaks attributed to GdOCl are also observed. At 800 °C, reflections from Gd_2O_3 and GdOCl are much enhanced whereas (00l) reflections of LGdH completely disappear. The single phase of Gd_2O_3 is formed at 850 °C, implying GdOCl exists within the narrow temperature range between 700 and 850 °C in atmospheric air. It is noted that the characteristic of layered structure is maintained up to at least 600 °C whereas the intralayer arrangement of LGdH is largely variable depending on temperature because of the easy deformation of hydroxyl groups. In general, (00l) reflections of layered materials appear in the low angle region (2θ < ~30°) and depend on the size of intercalated anion. If the neighboring layers are slipped sideways relative to each other, the sawtooth shaped feature is induced for ($h0l$)/(0kl) reflection family in the midangle region.[14] This phenomenon, called "turbostratic disorder" has been reported for transition metal hydroxides,[15] layered double

dx.doi.org/10.1021/ic301143r | Inorg. Chem. 2012, 51, 10222–10232

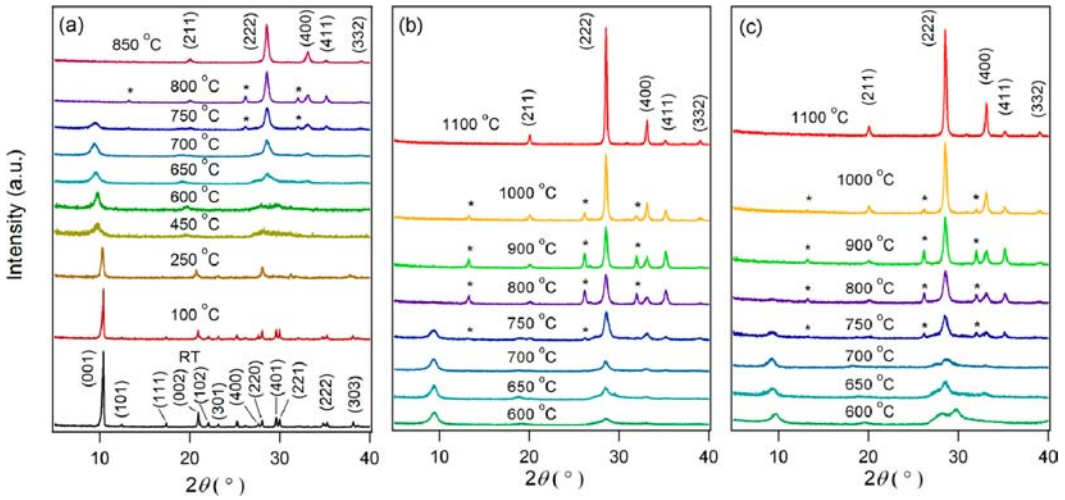

Figure 2. Powder XRD patterns of as-synthesized LGdH and its products after heating at 100−850 °C in atmospheric air (a) and 600−1100 °C under dry air (b) and Ar flow (c). Selected (*hkl*) assignments for the patterns obtained at RT and after heat treatment at higher than 800 °C are based on those of $Gd_2(OH)_5Cl{\cdot}nH_2O$ and Gd_2O_3, respectively. The reflections marked with an * correspond to those from GdOCl.

hydroxides (LDHs),[16] hydroxynitrates,[17] hydroxyacetates,[18] graphites,[19] graphens,[20] carbon nitrides,[21] boron nitrides.[22] In our study, powder XRD patterns of LGdH-450 and LGdH-600 show such a typical sawtooth shape in the 2θ range 25−40° (Figure 2a), because heating and natural cooling process could introduce an incomplete stacking of layers perpendicular to the *c*-axis. In contrast to conventional LDHs, LGdH did not show the turbostratic effect between RT and 250 °C. This difference implies that the guest species between inorganic sheets are better ordered in LGdH than in LDHs. The sawtooth shaped reflections weaken above 600 °C in accordance with the formation of Gd_2O_3 and GdOCl.

XRD patterns of LGdHs calcined at various temperatures in dry air are compared in Figure 2b. It is of interest that a considerable amount of GdOCl is still observed as a mixture with Gd_2O_3 even after heating LGdH at 1000 °C. Similar XRD patterns are observed during the calcination of LGdH under Ar flow as shown in Figure 2c. Reflections due to GdOCl disappear above 1100 °C in both environments. Figure 3 shows the thermogravimetry and differential thermogravimetry (TG-DTG) curves of LGdH under the different atmospheric conditions. TG and DTG thermograms from RT to around 580 °C overlap well, regardless of the nature of the environment. In dry air or Ar gas, weight loss continues up to around 1300 °C (end point: 1282 °C in dry air whereas slight above 1300 °C in Ar). In contrast, the decomposition of LGdH under atmospheric air is nearly completed at 1050 °C. This suggests that the thermal behavior of LGdH is strongly influenced by the environmental gases, which is consistent with the difference observed in XRD patterns (Figure 2).

To understand the thermal decomposition behavior of LGdH, the temperature-dependent gases that evolved were monitored by mass spectrometry. Figure 4 represents TG-

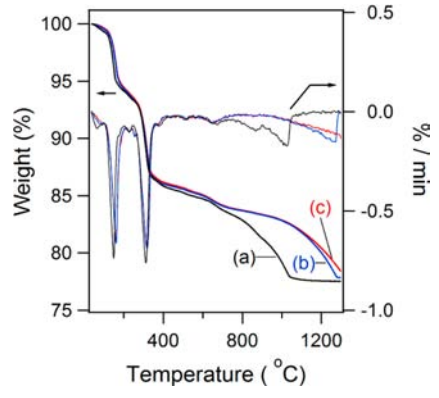

Figure 3. TG and DTG thermograms of LGdH in atmospheric air (a), dry air (b), and Ar gas (c).

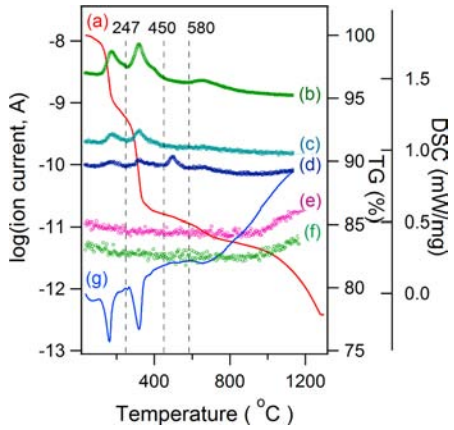

Figure 4. TG-DSC-MS curves of LGdH under dry air flow. TG (a) and DSC (g) data are adjusted to fit on MS data for comparison with each other. The ion currents of H_2O^+ (b), H^+ (c), CO_2^+ (d), $H^{35}Cl^+$ (e), and $H^{37}Cl^+$ (f) are plotted in log scale.

DSC-MS curves for the ions obtained when LGdH was heated in dry air up to 1300 °C. The mass spectra reveal temperature-dependent signals at various mass to charge ratios (*m*/*z*). The signals at *m*/*z* = 1, 18, 36, 38, and 44 correspond to the ionic peaks of H^+, H_2O^+, $H^{35}Cl^+$, $H^{37}Cl^+$, and CO_2^+, respectively. The weak CO_2 signal (Figure 4d) at high temperatures (450−800 °C) indicates that, as frequently observed in layered compounds such as LDHs, the carbonate anion can be incorporated into the interlayer galleries of LGdH as an impurity anion. Accordingly, the practical chemical formula of LGdH at RT is postulated as $[Gd_2(OH)_5]^+Cl^-_x(CO_3^{2-})_y{\cdot}nH_2O$ ($x + 2y = 1$).

dx.doi.org/10.1021/ic301143r | *Inorg. Chem.* 2012, 51, 10222−10232

Five steps of weight loss are monitored with the variation of ion currents due to the liberation of water, CO_2, and HCl molecules. The water and CO_2 loosely bound to the surface of bulk LGdH are desorbed at relatively low temperature. Because of the liberation of these water and CO_2 molecules, the ion currents of H_2O^+ (Figure 4b) and CO_2^+ (Figure 4d) decrease gradually when LGdH is heated from RT to around 100 °C.

$$[Gd_2(OH)_5]^+Cl^-_x(CO_3^{2-})_y\cdot nH_2O\cdot\{m_1CO_2\cdot m_2H_2O\} \rightarrow [Gd_2(OH)_5]^+Cl^-_x(CO_3^{2-})_y\cdot nH_2O + m_1CO_2 + m_2H_2O$$

At higher temperature, the ion currents of H_2O^+ and CO_2^+ increase simultaneously and peaked around 160 °C (Figures 4b and d). These signals are due to the dehydration of interlayer water molecules and the partial decarbonation of CO_3^{2-} ions cointercalated in the interlayer space of LGdH, resulting in the following weight loss (eq 1).

$$[Gd_2(OH)_5]^+Cl^-_x(CO_3^{2-})_y\cdot nH_2O \rightarrow [Gd_2(OH)_5]^+Cl^-_xO^{2-}_{y1}(CO_3^{2-})_{y-y1} + y_1CO_2 + nH_2O \quad (1)$$

Such dehydration and decarbonation processes terminate at around 247 °C. The H^+ ions (Figure 4c) originate from the thermal evolution of water molecules and shows the temperature dependence similar to that of H_2O^+ ion current (Figure 4b).

The second weight loss observed at 247−450 °C is mainly associated with the dehydroxylation of $[Gd_2(OH)_5]^+$ layers and partially with an additional decarbonation process (eq 2).

$$[Gd_2(OH)_5]^+Cl^-_xO^{2-}_{y1}(CO_3^{2-})_{y-y1} \rightarrow [Gd_2O_3H]^+Cl^-_xO^{2-}_{y1+y2}(CO_3^{2-})_{y-y1-y2} + y_2CO_2 + 2H_2O \quad (2)$$

Dehydroxylation induces the most drastic weight loss during the thermal decomposition of LGdH. Interestingly, between RT and 450 °C, the ionic current attributed to CO_2^+ molecules behaves essentially in accordance with that of H_2O^+. Because carbonate ions are co-intercalated with water molecules in the interlayer gallery, the void space produced by dehydration and dehydroxylation could act as the passageway for CO_2 molecules from the interlayer sites. This correlation seems to synchronize the decarbonation with the evolution of water molecules and to be responsible for the first decarbonation at low temperature (centered at 160 °C).[23]

The third step (450−580 °C) is characterized by a distinguishable ionic current of CO_2^+ peaked around 520 °C, without coupling with the behavior of H_2O^+ (eq 3, $y_1 + y_2 + y_3 + y_4 = y$).

$$[Gd_2O_3H]^+Cl^-_xO^{2-}_{y1+y2}(CO_3^{2-})_{y-y1-y2} \rightarrow [Gd_2O_3H]^+Cl^-_xO^{2-}_{y1+y2+y3}(CO_3^{2-})_{y4} + y_3CO_2 \quad (3)$$

This observation indicates that further heat treatment above 580 °C is required to completely remove the cointercalated carbonate. No signal related to HCl^+ was observed in the mass spectrometric data until this step.

In the fourth step (>580 °C), the final decarbonation (eq 4) and the second dehydroxylation occur along with the formation of Gd_2O_3 and GdOCl (eq 5). A broad weak ionic current of H_2O^+ (Figure 4b) is observed in the temperature between 580 and 850 °C and accompanied with a broad endothermic weight loss centered at 675 °C (Figures 4a and 4g). Carbonate ions survive in LGdH layers even up to 700 °C (Figure 4d), which is comparable with the complete decomposition of $Gd_2(CO_3)_3$ and $Gd_2(OH)_2(CO_3)_2$ into Gd_2O_3 at 700 and 720 °C, respectively.[24]

$$[Gd_2O_3H]^+Cl^-_xO^{2-}_{y1+y2+y3}(CO_3^{2-})_{y4} \rightarrow [Gd_2O_3H]^+Cl^-_xO^{2-}_y + y_4CO_2 \quad (4)$$

$$[Gd_2O_3H]^+Cl^-_xO^{2-}_y \rightarrow (1 - x/2)Gd_2O_3 + xGdOCl + (1/2)H_2O \quad (5)$$

The formation of GdOCl above 700 °C (Figure 2) causes the second dehydroxylation, supporting eq 5. As GdOCl shows a different reactivity against H_2O and O_2 molecules, the different decomposition processes are developed above 580 °C depending upon the environmental conditions.

The final step corresponds to the process to form a single phase of Gd_2O_3 together with the conversion of GdOCl to Gd_2O_3 (Supporting Information, Figure S2). In atmospheric air containing H_2O in proportion to the humidity, GdOCl readily reacts with H_2O molecules to form Gd_2O_3 with the liberation of HCl (eq 6).

$$GdOCl + (1/2)H_2O \rightarrow (1/2)Gd_2O_3 + HCl \quad (6)$$

Combining eq 5 and eq 6 gives ($x + 2y = 1$)

$$[Gd_2O_3H]^+Cl^-_xO^{2-}_y \rightarrow Gd_2O_3 + xHCl + yH_2O \quad (7)$$

In this condition, GdOCl is observed only between 700 and 850 °C in XRD patterns. Owing to the presence of relatively sufficient water molecules in atmospheric air, TG weight loss is significant below 1030 °C (Figure 3a and Supporting Information, Figure S1).

Under dry air or Ar flows, water molecules produced in eq 5 might be partially removed by flowing gas, so that the remaining water acts as the limiting agent in the thermal reaction of GdOCl ($x > x'$).

$$x'GdOCl + (x'/2)H_2O \rightarrow (x'/2)Gd_2O_3 + x'HCl \quad (6')$$

Combining eq 5 and eq 6′ gives

$$[Gd_2O_3H]^+Cl^-_xO^{2-}_y \rightarrow [1 - (x - x')/2]Gd_2O_3 + (x - x')GdOCl + x'HCl + [(1 - x')/2]yH_2O \quad (7')$$

This suggests that decomposition of $[Gd_2O_3H]^+Cl^-_xO^{2-}_y$ and conversion of GdOCl into Gd_2O_3 will proceed slowly because the amount of water is not sufficient. Gradual weight loss between 580 and 1000 °C (Figures 3b and 3c) could be correlated to such a slow conversion. As a result, (*hkl*) reflections of GdOCl are observed in XRD patterns of the samples calcined between 700 and 1000 °C both in dry air and Ar. Furthermore, GdOCl has another decomposition pathway into Gd_2O_3 in dry air as follows.

dx.doi.org/10.1021/ic301143r | *Inorg. Chem.* 2012, 51, 10222−10232

$$GdOCl + (1/4)O_2 \rightarrow (1/2)Gd_2O_3 + (1/2)Cl_2$$

Thus, GdOCl can be more easily transformed into Gd_2O_3 in dry air than in Ar gas. It has been reported that, if GdOCl is heated under the oxygen partial pressure of 100, 75, 50, and 25%, the end point of weight loss on its TG curve increases from 1161 °C to 1172, 1187, and 1209 °C, respectively.[25] Such a variation could explain why the weight loss of LGdH completes around 1282 °C in dry air whereas above 1300 °C under Ar flow (Figure 3). Equation 5 is then expressed as

$$[Gd_2O_3H]^+Cl^-_xO^{2-}_y + (x/4)O_2 \rightarrow Gd_2O_3 + (x/2)Cl_2 + (1/2)H_2O$$

Unfortunately, a signal due to Cl^+ (m/z = 35 and 37) or Cl_2^+ (m/z = 70, 72, and 74) was not detected in the mass spectra and therefore this process was not confirmed in our study. Nevertheless, considering that the weight loss is faster in dry air than in Ar above 1000 °C (Figures 3b and 3c) and signals due to HCl^+ (m/z = 36 and 38) are monitored (Figures 4e and 4f), a decomposition process catalyzed by oxygen molecules in dry air can be proposed (eq 8; $x + 2y = 1$).

$$[Gd_2O_3H]^+Cl^-_xO^{2-}_y + nO_2 \rightarrow Gd_2O_3 + xHCl + yH_2O + nO_2 \quad (8)$$

To sum up, TG curves of LGdH are well overlapped from RT to 580 °C regardless of the atmosphere. In the fourth step (580−800 °C in atmospheric air; 580−1000 °C in dry air or Ar gas), the intermediate $[Gd_2O_3H]^+Cl^-_xO^{2-}_y$ is transformed into Gd_2O_3 and GdOCl simultaneously. The atmosphere dependence observed in the decomposition of $[Gd_2O_3H]^+Cl^-_xO^{2-}_y$ results from the different reactivity of GdOCl toward H_2O and O_2 molecules. Hence, GdOCl and H_2O are key materials to understand the thermal decomposition mechanism of LGdH.

3.2. Estimation of the Composition. Using the TG-DTG-DSC data carried out in atmospheric air, we have tried to estimate the composition of LGdH. $[Gd_2O_3H]^+Cl^-_xO^{2-}_{y1+y2+y3}(CO_3^{2-})_{y4}$ intermediate at 580 °C is assumed to be equal to $[Gd_2O_3H]^+Cl^-_xO^{2-}_y$ because it is impossible to determine each y_i value due to the lack of structural information and y_4CO_2 is a tiny amount. Using eq 9 and eq 10, the composition of $[Gd_2(OH)_5]^+Cl^-_x(CO_3^{2-})_y{\cdot}nH_2O$ is estimated as follows: n = 1.67, x = 0.92 and y = 0.04 (Supporting Information).

$$\Delta W(RT - 580\ °C)/W_T = \{(2 + n)H_2O + yCO_2\}/W_T = 14.48\% \quad (9)$$

$$\Delta W(580 - 1400\ °C)/W_T = \{yH_2O + xHCl\}/W_T = 7.35\% \quad (10)$$

, where ΔW(RT−580 °C), ΔW(580−1400 °C), and W_T stand for the weight loss between the corresponding temperatures and the total weight of LGdH-RT, respectively. ΔW(RT−580 °C) is exclusively affected by dehydroxylaton and dehydration ($3.67H_2O$:$0.04\ CO_2$ = 38:1 in weight), whereas ΔW(580−1400 °C) is influenced nearly almost by the liberation of HCl ($0.04H_2O$:0.92HCl = 1:47 in weight).

$$\Delta W(RT - 580\ °C) = 3.67H_2O + 0.04CO_2 \approx 3.67H_2O$$

$$\Delta W(580 - 1400°C) = 0.04H_2O + 0.92HCl \approx 0.92HCl$$

Above 580 °C, the weight loss in atmospheric air proceeds with the formation of Gd_2O_3 and GdOCl and accelerates between 850 and 1030 °C with the liberation of HCl (eq 7 or eq 10). In this temperature range, Gd_2O_3 exist as the cubic phase with the space group of $Ia3$. Above 1030 °C, crystallization continues gently and a transition to the monoclinic phase ($C2/m$) takes place at 1200 °C.[26]

3.3. FT-IR characteristics. Thermochemical changes during the decomposition of LGdH were also investigated by FT-IR spectroscopy. Figure 5 compares FT-IR spectra of

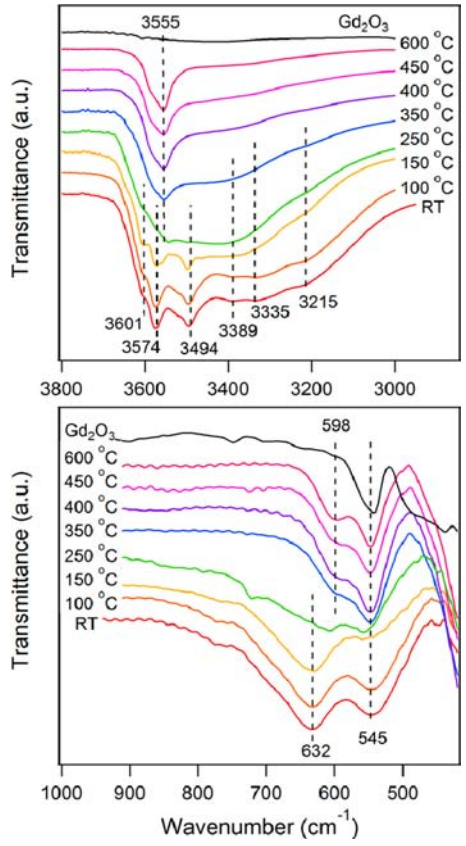

Figure 5. FT-IR spectra of LGdH and Gd_2O_3 in the range of 3800−2800 cm^{-1} (top) and 1000−400 cm^{-1} (bottom) as a function of calcination temperature.

LGdH before and after calcination at various temperatures. The stretching vibration mode of hydroxyl group in the inorganic matrix is generally observed between 3200 and 3700 cm^{-1}.[27] A broad band in the RT spectra consisting of fine structures at 3601, 3574, 3494, 3389, and 3335 cm^{-1} is accordingly attributed to the O−H stretching vibrations of intralayer hydroxyl groups and hydrogen-bonded interlayer water molecules. Fine structures at 3601, 3574, and 3494 cm^{-1} remain observable after calcining LGdH at 250 °C, whereas bands at 3389 and 3335 cm^{-1} are indistinguishable when heated at 150 °C. Judging from the fact that the dehydration of LGdH starts below 150 °C in the mass spectrometry data (Figure 4), the former three bands and the latter two bands could be assigned to the stretching vibrations of intralayer hydroxyl groups and interlayer water molecules, respectively.

dx.doi.org/10.1021/ic301143r | Inorg. Chem. 2012, 51, 10222−10232

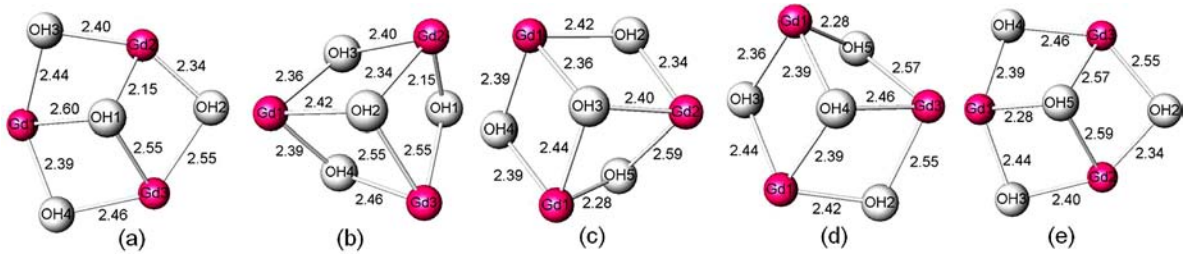

Figure 6. Length of Gd−O bonds surrounding μ_3-OH bonds in the lattice of LGdH. The relative strength of O−H bonds can be estimated by the average length of competing Gd−O bonds.

Table 1. Estimation of μ_3-OH Bond Strength in LGdH

	d_i	d_j	d_k	$d_i^2+d_j^2+d_k^2$	$\sqrt{(d_i^2+d_j^2+d_k^2)}$	O−H bond strength[a]
μ_3-OH1	2.15	2.55	2.60	17.89	4.23	2 (3574 cm^{-1})
μ_3-OH2	2.34	2.42	2.55	17.83	4.22	2 (3574 cm^{-1})
μ_3-OH3	2.36	2.40	2.44	17.28	4.16	3 (3494 cm^{-1})
μ_3-OH4	2.39	2.39	2.46	17.48	4.18	3 (3494 cm^{-1})
μ_3-OH5	2.28	2.57	2.59	18.51	4.30	1 (3601 cm^{-1})

[a]The ranks of μ_3-OH bond strength. Equivalent O−H stretching vibrations are given in parentheses.

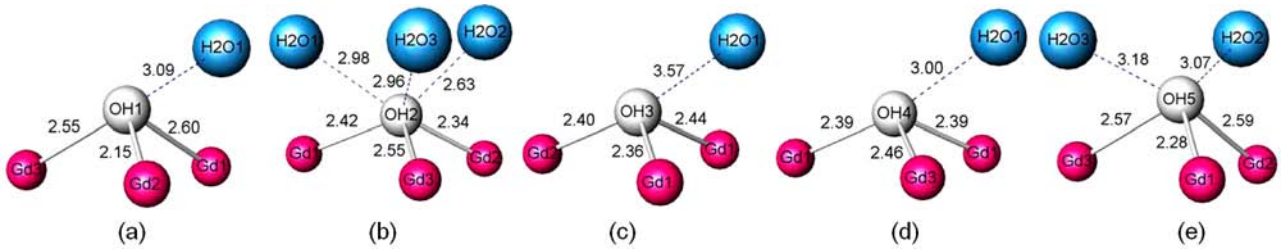

Figure 7. Local environment for μ_3-OH bonds in the lattice of LGdH. The O−H2 bond can be surrounded by three water molecules as the nearest neighbors, whereas other O−H bonds have one or two water molecules at long distances so that they are less influenced by the interlayer hydrogen bonding.

Bands at 3601, 3574, and 3494 cm^{-1} converge into a unique band around 3555 cm^{-1} as a result of dehydroxylation at temperatures higher than 350 °C. This band persists even after heating at 600 °C. It has been reported that the OH groups in Gd_2O_3 film fabricated by the sol−gel process still exist at 750 °C, but they almost disappear when the temperature reaches 900 °C.[28]

According to the structural data for LGdH,[4e] Gd^{3+} cations occupy the eight-coordinated polyhedral site (Gd1) and two types of nine-coordinated polyhedral sites (Gd2 and Gd3). The polyhedra are then linked to one another by five types of μ_3-OH groups (OH1, OH2, OH3, OH4, and OH5), providing three kinds of crystallographic sites partially occupied by the interlayer water molecules (H_2O1, H_2O2, and H_2O3). The μ_3-OH group is frequently found in natural hydroxides, including $Mg(OH)_2$ brucite and $Al(OH)_3$ gibbsite. Brucite has the hexagonal structure of $D^3_{3d}(P\bar{3}m)$ space group. Factor group analysis of $Mg(OH)_2$ showed two internal O−H vibrations, the A_{1g} Raman active mode and the A_{2u} IR active mode at 3655 and 3700 cm^{-1}, respectively.[29] $Al(OH)_3$ contains six nonequivalent OH groups, exhibiting six-forked O−H stretching bands at 3621, 3526, 3514, 3455, 3394, and 3373 cm^{-1} in IR spectra and at 3623, 3526, 3519, 3433, 3370, and 3363 cm^{-1} in Raman spectra.[30] In the structure of LGdH, the stretching vibration of μ_3-OH bonds is influenced by both neighboring hydroxyl groups and water molecules. Fine structures observed in the O−H stretching vibration range (3800−3400 cm^{-1}) of FT-IR spectra (Figure 5(top)) would be associated with the different μ_3-bonding environment, as shown in Figure 6. The three-forked (3601, 3574, and 3494 cm^{-1}) O−H stretching vibrations in IR spectra of LGdH-RT are explained by three average Gd−O bond distances. The estimated ranks of μ_3-OH bond strengths are listed in Table 1. The symbols of d_i, d_j, and d_k represent the bond lengths between Gd and μ_3-O atoms in Figure 6. It is generally accepted that the stronger Gd−O bond will result in the weaker competing O−H bond in the Gd_3OH tetrahedron. The smaller value of $\sqrt{(d_i^2 + d_j^2 + d_k^2)}$ represents the higher average strength of the Gd−O bonds, which will weaken the competing O−H bond to lower the vibrational frequency. It is consequently proposed that a strong shoulder band observed at 3601 cm^{-1} corresponds to the stretching vibration of the μ_3-OH5 bond, and the band at 3574 cm^{-1} with a weak shoulder corresponds to the vibrations of the μ_3-OH1 and μ_3-OH2 bonds. The band at 3494 cm^{-1}, which also includes a shoulder, is then assigned to the μ_3-OH3 and μ_3-OH4 bonds.

As depicted in Figure 7, the μ_3-OH2 hydroxyl group can be surrounded by up to three water molecules at relatively short distances, and is expected to be significantly influenced by the hydrogen bonding. In contrast, other μ_3-hydroxyl groups form hydrogen bonds with only one or two water molecules at relatively large distances. Essentially no hydrogen bonding is expected between the μ_3-OH3 and the interlayer water molecules. The different surroundings of the μ_3-OH bonds affect their hydrogen bonding with interlayer water molecules and are responsible for the weak shoulders in the fine structure.

dx.doi.org/10.1021/ic301143r | Inorg. Chem. 2012, 51, 10222−10232

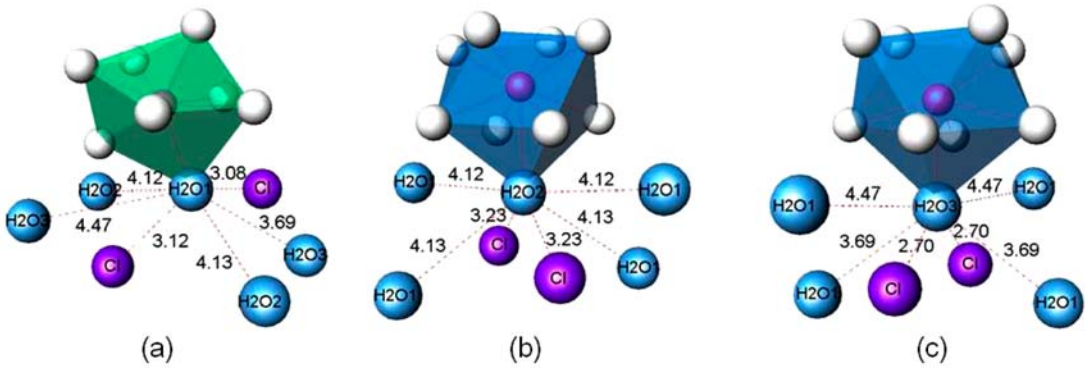

Figure 8. Local environments of three crystallographic sites for water molecules in the interlayer space of LGdH. Low occupancy is expected for the H_2O3 site because of the small distance between H_2O3 and Cl.

Figure 8 schematically represents three possible crystallographic sites for water molecules in the interlayer space of LGdH. Every site is partially occupied by water molecules and is ideally surrounded by four neighboring water molecules and two trans-type Cl atoms. However, the H_2O3 site is expected to have low occupancy because of the short distance between the water molecule and the Cl atom. Consequently, only two types of water molecules, H_2O1 and H_2O2, are practically defined in LGdH. The broad bands at 3389 and 3335 cm^{-1} in Figure 5a are assigned to these interlayer water molecules. This picture supports the significant weakening of these bands at temperatures higher than 150 °C. The broad shoulder around 3215 cm^{-1} is likely ascribed to the water molecules that are hydrogen bonded in the interlayer, as observed in FT-IR spectra of classical LDHs.[27,31] This band becomes considerably weaker at around 150 °C and disappears above 350 °C, when the hydrogen bonding system is destroyed. In Figure 5 (bottom), IR spectra of heat-treated LGdHs are compared in 1000−400 cm^{-1} range. At RT, the band at 632 cm^{-1} corresponds to the librational mode of water,[32,33] and the bands at 545 cm^{-1} are due to ν(Gd−O) stretching vibration in the $[Gd_2(OH)_5]^+$ layers.[34] As the dehydration proceeds in LGdH, the 632 cm^{-1} band gradually weakens and disappears around 250 °C. A new band around 598 cm^{-1}, which is developed above 250 °C and enhanced up to 600 °C, is assigned to the librational mode of O−H bond[35] in $[Gd_2O_3H]^+$ layers. This band behaves synchronously with the O−H stretching mode at 3555 cm^{-1}, formed as a result of dehydroxylation. In contrast, the band at 545 cm^{-1} due to ν(Gd−O) vibration is maintained up to 600 °C at least, which is compatible with the fact that (00*l*) reflections are still observed at this temperature. This implies that the Gd−O networks in the host layers are well reserved despite dehydroxylation.

3.4. Recovery of the Intercalation Ability of Calcined LGdHs. Because characteristic (00*l*) reflections of a layered structure were observed even after heating LGdH at 600 °C (Figure 2), the intercalation reactions of organic anions were carried out with LGdHs calcined at 450 and 600 °C. Interestingly, despite the maintenance of a layered structure, the intercalation behaviors of calcined LGdHs differed depending on the degrees of rehydration and rehydroxylation of the layers. Figure 9 compares XRD patterns of LGdH-450 (LGdH calcined at 450 °C) before and after the anion exchange reactions in aqueous octanesulfonate ($C_8H_{17}SO_3^-$) solution at RT and 60 °C. As shown in Figure 9b, the XRD pattern of LGdH-450 exhibits no change after reacting at RT for 24 h, indicating no intercalation of octanesulfonate anion. In

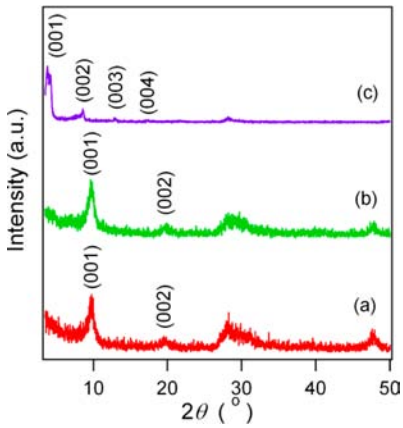

Figure 9. XRD patterns of LGdH-450 before (a) and after the exchange **reaction** in aqueous octanesulfonate solution at RT for 24 h (b) and at 60 °C for 18 h (c).

contrast, a drastic change was induced after the exchange reaction of LGdH-450 at 60 °C for 18 h (Figure 9c). A systematic shift of intense basal (00*l*) reflections toward lower diffraction angles and disappearance of the turbostratic disorder evidently result from the expansion of interlayer separation to 20.7 Å. This basal spacing is consistent with that of $Gd_2(OH)_5(C_8H_{17}SO_3)\cdot 1.5H_2O$, which was obtained through the exchange reaction of $Gd_2(OH)_5NO_3\cdot H_2O$ in aqueous octanesulfonate solution at RT.[4c] Similar behavior was also observed with LGdH-600, whose XRD pattern exhibited layered characteristics (Supporting Information, Figure S3). These results demonstrate the incorporation of octanesulfonate anions into interlayer galleries, leading to the conclusion that the intercalation ability of LGdHs calcined below 600 °C can be recovered by an appropriate layer activation process. The reaction of LGdH-700, which contained a considerable amount of Gd_2O_3 phase (Figure 2), was not completed after 18 h at 60 °C (Supporting Information, Figure S4). No difference was observed in the XRD patterns before and after the exchange reaction with LGdH-750, which had essentially no layered character (Supporting Information, Figure S5).

When hydrated in solution containing a given anion, calcined LDHs can recover their layered structures.[36] This interesting phenomenon has been adopted as a facile route to prepare pillared LDHs by exposing calcined LDHs to the appropriate organic or inorganic anion solutions.[37] Such a "memory effect" of LDHs calcined to a mixture of metal oxides is different from the recovery behavior of LGdH. Even though layered

dx.doi.org/10.1021/ic301143r | *Inorg. Chem.* 2012, 51, 10222−10232

characteristics are maintained in LGdH-450 and LGdH-600, an activation process at temperatures higher than RT (e.g., 60 °C) is required to recover the anion intercalation ability. Furthermore, the intercalation ability was not recovered when LGdH is calcined to Gd_2O_3. To assess the effect of temperature on the activation process required for recovering intercalation ability, LGdHs calcined at 350, 450, and 600 °C were placed in water with no counteranions and kept in air at RT for 24 h and at 60 °C for 18 h. FT-IR spectra of LGdH-450 are compared with those of its water treated products in Figure 10. Essentially

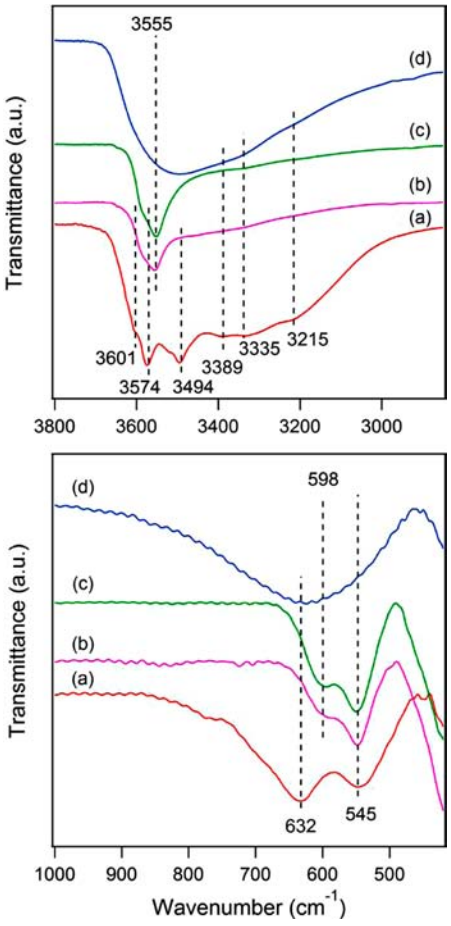

Figure 10. FT-IR spectra of LGdH-RT (a) and LGdH-450 before (b) and after rehydration and rehydroxylation in water at RT for 24 h (c) and at 60 °C for 18 h (d).

no difference is observed between IR spectra measured before and after water treatment at RT (Figures 10b and 10c), which indicate that no additional hydration or hydroxylation occurred at RT. If we consider that very fast rehydration and reconstruction have been observed upon exposure of calcined LDHs to air,[36,38] calcined LGdH appears much more stable than calcined LDHs in air, despite having the similar structure. The IR spectrum measured after water treatment at 60 °C (Figure 10d) is significantly different from that of LGdH-450 but instead, roughly comparable to that of LGdH-RT, shown in Figure 10a. The broad band of strongly increased intensity around 3389, 3335, and 3215 cm^{-1} indicates the reconstruction of the hydrogen bonding system by rehydration of the interlayer space. The enhancement in intensity around 3601, 3574, and 3494 cm^{-1} results from the rehydroxylation of the calcined LGdH layer. The strong band around 632 cm^{-1} after water treatment at 60 °C supports the change of interlayer structure due to rehydration. These changes in IR spectra suggest the regeneration of LGdH structure accompanied with the modification in intralayer arrangement of LGdH-450. Similar change was induced with LGdH-350, which had an IR spectrum similar to that of LGdH-450 (Supporting Information, Figure S6). It is accordingly concluded that the ability of calcined LGdHs to intercalate anions into their interlayer spaces is recovered by the reconstruction of interlayer structure through rehydration and rehydroxylation. These processes are significantly accelerated at the elevated temperature.

3.5. Dependence of the Recovery Behavior of Calcined LGdHs on the Counteranions in Aqueous Solution. Despite similar XRD patterns, IR spectra, and intercalation behaviors, the rehydration and rehydroxylation of LGdH-600 in water were quite different from those of LGdH-350 and LGdH-450. As shown in Figure 11d, no increase in

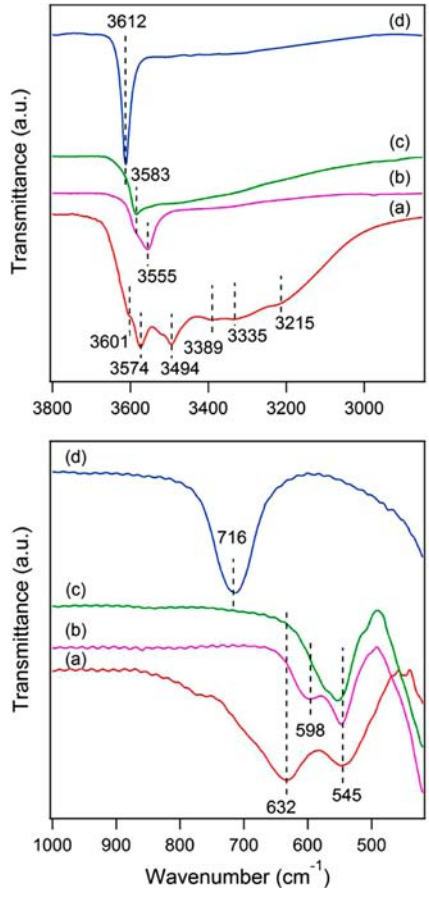

Figure 11. FT-IR spectra of LGdH-RT (a) and LGdH-600 before (b) and after rehydration and rehydroxylation in water at RT for 24 h (c) and at 60 °C for 18 h (d).

intensity of bands attributed to the rehydration (3389−3215 cm^{-1}), rehydroxylation (3601−3494 cm^{-1}), and reconstruction of intralayer structure (632−545 cm^{-1}) of LGdH-600 is induced even after water treatment at 60 °C for 18 h. Sharp single band at 3612 cm^{-1} and strong band at 716 cm^{-1}, which are identical to those of $Gd(OH)_3$ (Supporting Information, Figure S7), are clearly observed. Its XRD pattern shown in Supporting Information, Figure S8 confirmed the transformation of LGdH-600 to $Gd(OH)_3$ by water treatment at 60 °C.

dx.doi.org/10.1021/ic301143r | Inorg. Chem. 2012, 51, 10222−10232

If we recall that the intercalation ability of LGdH-600 was recovered in aqueous octanesulfonate solution at 60 °C (Supporting Information, Figure S3), a transformation to $Gd(OH)_3$ in water is seemingly contradictory. It has been known that experimental conditions strongly affect the ability of the metal oxide mixture, obtained after calcining LDHs, to recover the layered structure.[39] Therefore, we postulated that rehydration and rehydroxylation behaviors of calcined LGdHs could be different depending on the existence of counteranions in solution. To confirm this possibility, LGdH-600 was heated at 60 °C for 18 h in aqueous NaCl and $NaNO_3$ solutions. FT-IR spectra and XRD patterns of the resulting powders are compared in Figures 12 and 13, respectively. In contrast to the

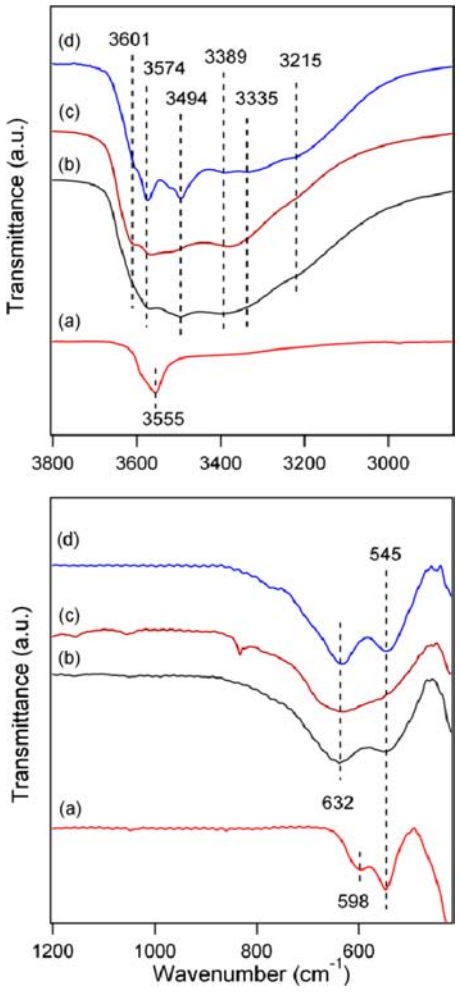

Figure 12. FT-IR spectra of LGdH-600 before (a) and after rehydration and rehydroxylation in aqueous solutions of NaCl (b) and $NaNO_3$ (c) at 60 °C for 18 h. (d) FT-IR spectrum of LGdH-RT for comparison.

spectrum measured after heating at 60 °C in water (Figure 11d), the appearance of strong broad band including the fine structures at 3700−2800 cm^{-1} and highly enhanced intensity around 632 cm^{-1} indicates that LGdH-600 was not transformed to $Gd(OH)_3$ at 60 °C. Instead, IR spectra of LGdH-600 after heating in aqueous NaCl and $NaNO_3$ solutions are quite similar to those of LGdH-RT. The sawtooth shaped reflections due to the turbostratic disorder are considerably relieved in XRD patterns (Figures 13b and c), implying that guest ions such as Cl^- and NO_3^- are fairly well ordered between the

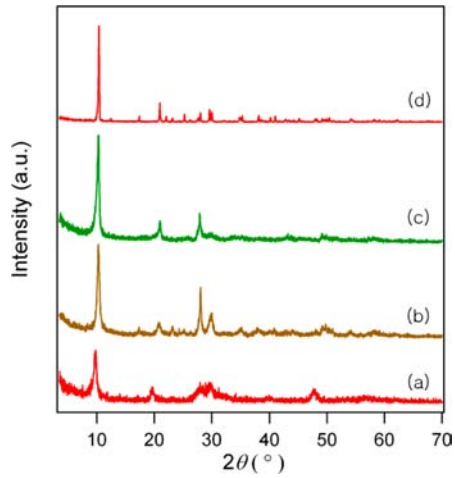

Figure 13. XRD patterns of LGdH-600 before (a) and after rehydration and rehydroxylation in aqueous solutions of NaCl (b) and $NaNO_3$ (c) at 60 °C for 18 h. (d) XRD pattern of LGdH-RT for comparison.

inorganic layers. Hence, it is evident that the intralayer structure of LGdH-600 was reconstructed by rehydration and rehydroxylation in aqueous solution containing inorganic counteranions at 60 °C.

Finally, it is remarked that, when rehydration and rehydroxylation were carried out at 100 °C in water without any counteranion, calcined LGdHs were transformed to $Gd(OH)_3$ regardless of calcination temperature. Conversely, the transformation of calcined LGdHs to $Gd(OH)_3$ was not induced if the aqueous solution contains organic or inorganic anions, even at 100 °C. Instead, the crystalinity of products obtained by the reconstruction of calcined LGdHs was highly improved. Thus, both the solution temperature and the presence of counteranions in solution have to be controlled for the reconstruction of calcined LGdHs.

4. CONCLUSIONS

We have systematically investigated the thermal behavior of layered gadolinium hydroxychloride, $Gd_2(OH)_5Cl{\cdot}nH_2O$ (LGdH), on the basis of combined analytical results of thermogravimetry-differential scanning calorimetry-mass spectrometry (TG-DSC-MS). When heated, LGdH decomposes into Gd_2O_3 and GdOCl, regardless of the atmospheric gas. However, the complete decomposition temperature of LGdH can differ by nearly up to 300 °C depending on the water content in atmosphere. Such different decomposition behaviors of LGdH result from the different reactivity of GdOCl toward H_2O and O_2 molecules. By rehydration and rehydroxylation in aqueous solution containing organic and inorganic anions, the intralayer structure of LGdHs calcined up to 600 °C can be reconstructed to recover the intercalation ability. The calcination temperature capable of reconstruction is quite high compared with those of classical LDHs. High thermal stability and reconstructability would provide the LRH family, including LGdH, with many advantages for high temperature applications.

■ ASSOCIATED CONTENT

Supporting Information

Further details are given in Figures S1−S8. This material is available free of charge via the Internet at http://pubs.acs.org.

dx.doi.org/10.1021/ic301143r | Inorg. Chem. 2012, 51, 10222−10232

AUTHOR INFORMATION

Corresponding Author

*E-mail: shbyun@khu.ac.kr (S.-H.B), spin9898@empas.com (J.-K.K).

Author Contributions

‖These authors equally contributed to the work.

Notes

The authors declare no competing financial interest.

ACKNOWLEDGMENTS

S.-H.B. acknowledges support from the Midcareer Researcher Program through National Research Foundation (NRF) grant funded by the Ministry of Education, Science and Technology (MEST) (No. 2012-0005305). J.-K.K. acknowledges support from the Priority Research Centers Program through National Research Foundation of Korea (No. 2009-0094046).

REFERENCES

(1) (a) Ma, R.; Liang, J.; Takada, K.; Sasaki, T. *J. Am. Chem. Soc.* **2011**, *133*, 613−620. (b) Ay, A. N.; Karan, B.; Temel, A.; Rives, V. *Inorg. Chem.* **2009**, *48*, 8871−8877. (c) Feng, L.; Duan, X. *Struct. Bonding (Berlin)* **2006**, *119*, 193−223 , and references therein.

(2) (a) Gago, S.; Pillinger, M.; Ferreira, R. A. S.; Carlos, L. D.; Santos, T. M.; Goncalves, I. S. *Chem. Mater.* **2005**, *17*, 5803−5809. (b) Li, C.; Wang, G.; Evans, D. G.; Duan, X. *J. Solid State Chem.* **2004**, *177*, 4569−4575. (c) Kaneyoshi, M.; Jones, W. *Mol. Cryst. Liq. Cryst.* **2001**, *356*, 459−468.

(3) Gandara, F.; Perles, J.; Snejko, N.; Iglesias, M.; Gomez-Lor, B.; Gutierrez-Puebla, E.; Monge, M. A. *Angew. Chem., Int. Ed.* **2006**, *45*, 7998−8001.

(4) (a) Lee, K.-H.; Byeon, S.-H. *Eur. J. Inorg. Chem.* **2009**, 4727−4732. (b) Geng, F.; Matsushita, Y.; Ma, R.; Xin, H.; Tanaka, M.; Iyi, N.; Sasaki, T. *Inorg. Chem.* **2009**, *48*, 6724−6730. (c) Lee, K.-H.; Byeon, S.-H. *Eur. J. Inorg. Chem.* **2009**, 929−936. (d) Poudret, L.; Prior, T. J.; McIntyre, L. J.; Fogg, A. M. *Chem. Mater.* **2008**, *20*, 7447−7453. (e) Geng, F.; Matsushita, Y.; Ma, R.; Xin, H.; Tanaka, M.; Izumi, F.; Iyi, N.; Sasaki, T. *J. Am. Chem. Soc.* **2008**, *130*, 16344−16350. (f) McIntyre, L. J.; Jackson, L. K.; Fogg, A. M. *Chem. Mater.* **2008**, *20*, 335−340.

(5) (a) Yoon, Y.-S.; Byeon, S.-H.; Lee, I. S. *Adv. Mater.* **2010**, *22*, 3272−3276. (b) Ida, S.; Sonoda, Y.; Ikeue, K.; Matsumoto, Y. *Chem. Commun.* **2010**, *46*, 877−879. (c) Lee, K.-H.; Lee, B.-I.; You, J.-H.; Byeon, S.-H. *Chem. Commun.* **2010**, *46*, 1461−1463. (d) Hu, L.; Ma, R.; Ozawa, T. C.; Sasaki, T. *Angew. Chem., Int. Ed.* **2009**, *48*, 3846−3849.

(6) Geng, F.; Ma, R.; Sasaki, T. *Acc. Chem. Res.* **2010**, *43*, 1177−1185.

(7) Lee, B.-I.; Lee, K. S.; Lee, J. H.; Lee, I. S.; Byeon, S.-H. *Dalton Trans.* **2009**, 2490−2495.

(8) (a) Yoon, Y.-S.; Lee, B.-I.; Lee, K. S.; Heo, H.; Lee, J. H.; Byeon, S.-H.; Lee, I. S. *Chem. Commun.* **2010**, *46*, 3654−3656. (b) Yoon, Y.-S.; Lee, B.-I.; Lee, K. S.; Im, G. H.; Byeon, S.-H.; Lee, J. H.; Lee, I. S. *Adv. Funct. Mater.* **2009**, *19*, 3375−3380.

(9) (a) Lee, B.-I.; Lee, S.-Y.; Byeon, S.-H. *J. Mater. Chem.* **2011**, *21*, 2916−2923. (b) Xi, Y.; Davis, R. J. *Inorg. Chem.* **2010**, *49*, 3888−3895.

(10) Lee, B.-I.; Byeon, S.-H. *Chem. Commun.* **2011**, *47*, 4093−4095.

(11) (a) Han, F.; Teng, Q.; Zhang, Y.; Wang, Y.; Shen, Q. *Inorg. Chem.* **2011**, *50*, 2634−2643. (b) Zhou, S.; Wu, S.; Zhu, H.; Wang, S.; Zhu, X.; Zhang, L.; Yang, G.; Cui, D.; Wang, H. *Dalton Trans.* **2011**, *40*, 9447−9453. (c) Dang, D.; Bai, Y.; He, C.; Wang, J.; Duan, C.; Niu, J. *Inorg. Chem.* **2010**, *49*, 1280−1282. (d) Snejko, N.; Cascales, C.; Gomez-Lor, B.; Gutierrez-Puebla, E.; Iglesias, M.; Ruiz-Valero, C.; Monge, M. A. *Chem. Commun.* **2002**, 1366−1367. (e) Mejia-Radillo, Y.; Yatsimirsky, A. K. *Inorg. Chim. Acta* **2002**, *328*, 241−246.

(12) Hu, L.; Ma, R.; Ozawa, T. C.; Sasaki, T. *Inorg. Chem.* **2010**, *49*, 2960−2968.

(13) When deposited to form (ultra) thin films on a substrate, $Gd_2(OH)_5Cl{\cdot}nH_2O$ transforms to Gd_2O_3 at 600 °C. Lee, B.-I.; Lee, E.-s.; Byeon, S.-H. *Adv. Funct. Mater.* **2012**, *22*, 3562−3569.

(14) Thomas, G. S.; Kamath, P. V. *J. Chem. Sci.* **2006**, *118*, 127−133.

(15) (a) Ramesh, T. N.; Kamath, P. V. *Mater. Res. Bull.* **2008**, *43*, 3227−3233. (b) Arulraj, J.; Rajamathi, J. T.; Prabhu, K. R.; Rajamathi, M. *Solid State Sci.* **2007**, *9*, 812−816. (c) Wang, C. Y.; Zhong, S.; Konstantinov, K.; Walter, G.; Liu, H. K. *Solid State Ionics* **2002**, *148*, 503−508. (d) Delahaye-Vidal, A.; Figlarz, M. *J. Appl. Electrochem.* **1987**, *17*, 589−599.

(16) (a) Radha, A. V.; Thomas, G. S.; Kamath, P. V.; Antonyraj, C. A. *Bull. Mater. Sci.* **2010**, *33*, 319−324. (b) Cui, G.; Evans, D. G.; Li, D. *Polym. Degrad. Stab.* **2010**, *95*, 2082−2087. (c) Scheinost, A. C.; Spark, D. L. *J. Colloid Interface Sci.* **2006**, *294*, 234−239.

(17) Rajamathi, M.; Kamath, P. V. *Int. J. Inorg. Mater.* **2001**, *3*, 901−906.

(18) (a) Sicard, L.; Ammar, S.; Herbst, F.; Mangeney, C.; Fievet, F.; Viau, G. *Mater. Res. Bull.* **2009**, *44*, 1692−1699. (b) Rajamathi, J. T.; Ahmed, M. F.; Ravishanker, N.; Nethravathi, C.; Rajamathi, M. *Solid State Sci.* **2009**, *11*, 1270−1274.

(19) (a) Zheng, T.; Reimers, J. N.; Dahn, J. R. *Phys. Rev.* **1995**, *51*, 734−741. (b) Hishiyama, Y.; Nakamura, M. *Carbon* **1995**, *33*, 1399−1403. (c) Biscoe, J.; Warren, B. E. *J. Appl. Phys.* **1942**, *13*, 364−371.

(20) Shibuta, Y.; Elliot, J. A. *Chem. Phys. Lett.* **2011**, *512*, 146−150.

(21) Solozhenko, V. L.; Solozhenko, E. G.; Zinin, P. V.; Ming, L. C.; Chen, J.; Parise, J. B. *J. Phys. Chem. Solids* **2006**, *67*, 932−937.

(22) (a) Guo, Q.; Xie, Y.; Yi, C.; Zhu, L.; Gao, P. *J. Solid State Chem.* **2005**, *178*, 1925−1928. (b) Alkoy, S.; Toy, C.; Gönül, T.; Tekin, A. *J. Eur. Ceram. Soc.* **1997**, *17*, 1415−1422.

(23) (a) Liang, L. V. *Desalination* **2007**, *208*, 125−133. (b) Hutson, N. D. *Chem. Mater.* **2004**, *16*, 4135−4143. (c) Yang, W.; Kim, Y.; Liu, P. K. T.; Sahimi, M.; Tsotsis, T. T. *Chem. Eng. Sci.* **2002**, *57*, 2945−2953. (d) Levedeva, O.; Tichit, D.; Coq, B. *Appl. Catal., A* **1999**, *183*, 61−71.

(24) Lechevallier, S.; Lecante, P.; Mauricot, R.; Dexpert, H.; Dexpert-Ghys, J.; Kong, H.-K.; Wong, K.-L. *Chem. Mater.* **2010**, *22*, 6153−6161.

(25) Yang, H. C.; Cho, Y. J.; Eun, H. C.; Kim, E. H.; Kim, I. T. *J. Therm. Anal. Calorim.* **2007**, *90*, 379−384.

(26) Balestrieri, D.; Philipponneau, Y.; Decroix, G. M.; Jorand, Y.; Fantozzi, G. *J. Eur. Ceram. Soc.* **1998**, *18*, 1073−1077.

(27) Nakamoto, K. *Infrared and Raman Spectra of Inorganic and Coordination Compounds: Theory and applications in inorganic chemistry*; John Wiley: New York, 1997.

(28) (a) Guo, H.; Yang, X.; Xiao, T.; Zhang, W.; Lou, L.; Mugnier. *J. Appl. Surf. Sci.* **2004**, *230*, 215−221. (b) McDevitt, N.; Davison, A. *J. Opt. Soc. Am.* **1966**, *56*, 636−638.

(29) Kruger, M. B.; Williams, O.; Jeanloz, R. *J. Chem. Phys.* **1989**, *91*, 5910−5915.

(30) Balan, E.; Lazzeri, M.; Morin, G.; Nauri, F. *Am. Mineral.* **2006**, *91*, 115−119.

(31) Bish, D. L.; Brindley, G. W. *Am. Mineral.* **1977**, *62*, 458−464.

(32) (a) Brubach, J.-B.; Mermet, A.; Filabozzi, A.; Gerschel, A.; Roy, P. *J. Chem. Phys.* **2005**, *122*, 184509. (b) Praprotnik, M.; Janezic, D.; Mavri, J. *J. Phys. Chem. A* **2004**, *108*, 11056−11062. (c) Zelsmann, H. R. *J. Mol. Struct.* **1995**, *350*, 95−114.

(33) (a) Palmer, S J.; Frost, R. L.; Nguyen, T. *Coor. Chem. Rev.* **2009**, *253*, 250−267. (b) Hofer, T. S.; Scharnagl, H.; Randolf, B. R.; Rode, B. M. *Chem. Phys.* **2006**, *327*, 31−42. (c) Maczka, M.; Hanuza, J.; Kaminskii, A. A. *J. Raman Spectrosc.* **2006**, *37*, 1257−1264. (d) Koleva, V. G. *Spectrochim. Acta A* **2005**, *62*, 1196−1202. (e) Kagunya, W.; Baddour-Hadjean, R.; Kooli, F.; Jones, W. *Chem. Phys.* **1998**, *236*, 235−234.

(34) Paul, N.; Devi, M.; Mohanta, D. *Mater. Res. Bull.* **2011**, *46*, 1296−1300.

(35) (a) Mu, Q.; Wang, Y. *J. Alloys Compd.* **2011**, *509*, 2060−2065. (b) Kaflak, A.; Kolodziejski, W. *J. Mol. Struct.* **2011**, *990*, 263−270. (c) Get'man, E. I.; Yablochkoba, N. V.; Loboda, S. N.; Prisedsky, V. V.; Antonovich, V. P.; Chivireva, N. A. *J. Solid State Chem.* **2008**, *181*,

2386−2392. (d) Nagao, M.; Hamano, H.; Hirata, K.; Kumashiro, R.; Kuroda, Y. *Langmuir* **2003**, *19*, 9201−9209.
(36) Constantino, V. R. L.; Pinnavaia, T. J. *Inorg. Chem.* **1995**, *34*, 883−892.
(37) (a) Ulibani, M. A.; Labajos, F. M.; Rives, V.; Trujillano, R.; Kagunya, W.; Jones, W. *Inorg. Chem.* **1994**, *33*, 2592−2599. (b) Chibwe, K.; Jones, W. *Chem. Mater.* **1989**, *1*, 489−490. (c) Chibwe, K.; Jones, W. *J. Chem. Soc., Chem. Commun.* **1989**, 926−927.
(38) Rey, F.; Fornes, V.; Rojo, J. M. *J. Chem. Soc. Faraday Trans.* **1992**, *88*, 2233−2238.
(39) Kooli, F.; Rives, V.; Ulibarri, M. A. *Mater. Sci. Forum* **1994**, *152*−*153*, 375−378.